Atomic Processes in Astrophysical Plasmas

Sultana N. Nahar
Dept of Astronomy, The Ohio State University, Columbus, OH 43210, USA

June 4, 2005

Abstract

Astrophysical plasmas either illuminated by radiative sources or dominated by electron collisions produce rich atomic spectra result from several dominant atomic processes: photoionization, electron-ion recombination, bound-bound radiative transitions, collisional excitations, and collisional ionizations. The absorption or emission line spectra enable determination of temperatures, densities, abundances of constituent elements and other macroscopic parameters of the astrophysical plasmas. Precise analysis of the spectra depends on accurate parameters for the atomic processes. Considerable progress in understanding the formation and structure of the astronomical objects has been made in the last few decades through high resolution spectra by ground and space based observatories and theoretical and computational advances. The major theoretical and computationanl advances have been under two international collaborations known as the Opacity Project (OP) and the Iron Project (IP) that have yielded accurate and large-scale atomic data for photoionization cross sections, radiative transition probabilities, and collision strengths for electron impact excitation for most astrophysically abundant atoms and ions, from hydrogen to iron and iron-peak elements. In addition a new theoretical unified method was developed to treat of the two inverse processes of photoionization and electron-ion recombination in a self-consistent manner. A brief description of the theoretical methodologies and results from the Ohio State atomic-astrophysics group as part of the OP and the IP collaborations are presented.

1 Introduction

The basic atomic processes that dominant the astrophysical plasmas are:

i) Radiative bound-bound transition for excitation and de-excitation:

$$X^{+Z} + h\nu \rightleftharpoons X^{+Z*},$$

where the ion, X, is of charge, Z. The atomic parameters of interest are the oscillator strengths (f) for excitation and the radiative decay rate or Einstein's coefficient for radiative transition probability (A-value) for de-excitation.

ii) Photoionization (PI) and radiative recombination (RR): In a single step process, an electron goes to continuum by absorption of a photon:

$$X^{+Z} + h\nu \rightleftharpoons X^{+Z+1} + \epsilon,$$

The inverse process is the radiative recombination (RR). These are non-resonant processes.

iii) Autoionization (AI) and dielectronic recombination (DR):

$$e + X^{+Z} \leftrightarrow (X^{+Z-1})^{**} \leftrightarrow \begin{cases} e + X^{+Z} & \text{AI} \\ X^{+Z-1} + h\nu & \text{DR} \end{cases}$$

In this two step process, the electron is colliding with an ion, excites the target as well as attaches itself to a highly excited level forming a doubly excited state, known as the autoionizing state. This state either leads to autoionization (AI), a radiationless process where the electron goes free and the target goes to ground state, or to dielectronic recombination (DR) when the electron is captured by emission of a photon. The inverse of DR is photoionization. Autoionizing states introduce resonances in atomic processes.

The atomic parameters of interest for photoionization and recombination process are the photoionization cross sections (σ_{PI}), recombination cross sections (σ_{RC}) and recombination rate coefficients (α_{RC}).

iv) The collisional process of electron-impact excitation (EIE) is

$$e + X^{+Z} \rightarrow e' + X^{+Z*}$$

This is one of the primary processes for spectral formation in astrophysical plasmas since the excited ion decays by emission of a photon. Collisional excitation may also go through an

intermediate doubly excited autoionizing states introducing resonances in the cross sections. The relevant atomic parameters of interest are collisional cross sections (σ_{EIE}) and the collision strengths (Γ).

v) The collisional process of electron-impact ionization is

$$e + X^{+Z} \rightarrow e' + e + X^{+(Z+1)}.$$

The atomic parameters of interest, ionization cross sections (σ) and collision strengths (S), for this process can be obtained experimentally more accurately than theoretical calculations and measured values are in general available. We are not concerned with this process at this time.

Each of the above processes needs to be treated separately to obtain the relevant parameters. Astrophysical model applications, such as determination of radiation transfer in plasmas for the opacities, need a large amount of atomic data as these deal with with many atomic levels and over a wide energy ranges. The Close Coupling (CC) R-matrix method employed by the Opacity Project (1995, 1996) and the Iron Project (Hummer et al. 1993) enable computation of such large scale atomic data. Work under these two projects have produced the detailed features of autoinizing resonances in the radiative and collisional processes for most of atoms and ions for the first time. The method enables self-consistent sets of atomic parameters if the atom or the ion is described by the same wavefunction expansion for each process. This reduces the uncertainty introduced in applications involving different processes and approximations.

The large amount of atomic data and plasma opacities obtained under the OP and the IP are available electronically from databases, such as TOPbase and TIPTOPBASE at CDS (Astronomy and Astrophysics Journal, France), Goddard-NASA, and the Ohio State University.

2 Theory

The R-matrix method in the close-coupling (CC) approximation (Burke & Robb 1975) is the most powerful method for ab initio atomic calculations. The entire region is divided in to two, the inner and the outer regions of of the R-matrix sphere with the atom or ion at the center. The inner region wavefunction is represented by a basis set known as the R-matrix basis. The size of the sphere is chosen such that the effects of the electron-electron correlation and other short-range

potentials is zero at the boundary. The method has been extended extensively under the OP for radiative processes (Seaton 1987, Berrington et al 1987, Nahar and Pradhan 1994a, 1995) and the IP for electron collisional as well radiative processes (Hummer et al. 1993, Berrington et al. 1995). Futher extension was made by developing the new unified treatment for total electron-ion recombination (Nahar and Pradhan 1992, 1994a). The computational packages of codes span a number of stages before obtaining the atomic parameters.

A brief summary of the theories to treat the atomic processes is given below.

a) The Hamiltonian

In non-relativistic atomic structure calculations, the energies and wavefunctions of an N-electron ion are obtained through optimum solution of the Schrodinger equation,

$$\left[\sum_{i=1}^{N}\left\{-\nabla_i^2 - \frac{2Z}{r_i} + \sum_{j>i}^{N}\frac{2}{r_{ij}}\right\}\right]\Psi = E\Psi, \tag{1}$$

where $\Psi = \Psi(\gamma SLM_S M_L|\mathbf{r}_1, ..., \mathbf{r}_N)$ are the bound solutions consisting of a linear combination of configuration state functions.

We include the relativistic effects through Breit-Pauli approximation. The approximation is more suitable for multi-electron systems than one-particle Dirac equations. The relativistic N-electron Hamiltonian in the Breit-Pauli (BP) approximation is (e.g. Eissner 1991)

$$H_{\rm BP} = H_{NR} + H_{\rm mass} + H_{\rm Dar} + H_{\rm so} +$$

$$\frac{1}{2}\sum_{i\neq j}^{N}[g_{ij}(so + so') + g_{ij}(ss') + g_{ij}(css') + g_{ij}(d) + g_{ij}(oo')], \tag{2}$$

where H_{NR} is the non-relativistic Hamiltonian, and

$$H_{\rm mass} = -\frac{\alpha^2}{4}\sum_i p_i^4\,, \qquad H_{\rm Dar} = -\tfrac{\alpha^2}{4}\textstyle\sum_i \nabla^2\left(\frac{Z}{r_i}\right), \qquad H_{\rm so} = \alpha^2\textstyle\sum_{i=1}\frac{Z}{r_i^3}{\rm l}(i)\cdot{\rm s}(i) \tag{3}$$

are the relativistic one-body mass correction, Darwin, and spin-orbit interaction terms. The rest are two-body interaction terms with notation c for contraction, d for darwin, o for orbit, s for spin and a prime indicates 'other'. The last three two-body terms very weak and may be igorned. The fine structure terms, that is spin-other-orbit (os') and spin-other-spin (ss') terms,

$$g_{ij}(so + so') = -\alpha^2(\frac{\mathbf{r}_{ij}}{r_{ij}^3}\times\mathbf{p}_i).(\mathbf{s}_i + 2\mathbf{s}_j) + (\frac{\mathbf{r}_{ij}}{r_{ij}^3}\times\mathbf{p}_j).(\mathbf{s}_j + 2\mathbf{s}_i)\,,$$

$$g_{ij}(ss') = 2\alpha^2 \frac{\mathbf{s}_i.\mathbf{s}_j}{r_{ij}^3} - 3\frac{(\mathbf{s}_i.\mathbf{r}_{ij})(\mathbf{s}_j.\mathbf{r}_{ij})}{r_{ij}^5} \tag{4}$$

together form the full Breit interaction term, $H^B = \sum_{i>j}[g_{ij}(so + so') + g_{ij}(ss')]$.

Spin-orbit interaction splits the LS terms into fine-structure levels labeled by $J\pi$ where J is the total angular momentum π is the parity. Rest of the relativistic terms improve the energy values and the wavefunctions. The electron-electron correlations contribute dominantly through *1/Z* dependence compared to the relativistic effects. Hence, in the Breit-Pauli R-matrix (BPRM) approximation, where correlation effects are treated more accurately, only the one-body relativistic terms are included.

However, for weak bound-bound radiative transitions of type intercombination and forbidden the relativistic corrections play an important role in distribution to fine structure components. The one-body terms vary as $\alpha^2 Z^4$ and contribute in general more than the two-body terms with one less power of Z. We include the contribution of the one-body terms and the full Breit interaction term for such transitions through atomic structure calculations.

b) Coupled Channel Wavefunction

The atomic system is represented by a coupled eigenfunction expansion in the close-coupling approximation. The ion or atom is treated as a (N+1) electron system where the core, called the "target" in CC approximation, has N number of electrons and the (N+1)th electron is the interacting electron which can be bound or in continuum. The total wavefunction of the (N+1) electron system is described as:

$$\Psi_E(e + ion) = A\sum_i^N \chi_i(ion)\theta_i + \sum_j c_j\Phi_j(e + ion), \tag{5}$$

where χ_i is the target ion or core wavefunction in a specific state $S_iL_i\pi_i$ or level $J_i\pi_i$, θ_i is the wavefunction of the interacting (N+1)th electron in a channel labeled as $S_iL_i(J_i)\pi_i\ k_i^2\ell_i(SL\pi\ or\ \ J\pi)$; k_i^2 is the incident kinetic energy. Φ_j is the correlation functions of (e+ion) system that compensates the orthogonality condition and short range correlation interations.

The complex resonant structures in photoionization, recombination, and in electron impact excitation are included through couplings of channels in Ψ_E. To each excited target state, there corresponds to a series of doubly excited states, $S_iL_i(J_i)\pi_i\nu l$, known as the Rydberg series, most

of which are autoionizing states as they lie above the ionizing potential and cause resonances. ν is the effective quantum number.

The wavefunction χ_i of the core or "target" is obtained through a configuration interaction atomic structure calculations before starting the R-matrix calculations. Most commonly used code for the purpose is SUPERSTRUCTURE (Eissner et al 1974, Eissner and Zeippen 1981, Eissner 1991, Nahar et al. 2003). The nuclear and electron-electron potential is represented by the statistical Thomas-Fermi-Dirac-Amaldi model potential $V^{SM}(r) = \frac{Z_{eff}(\lambda_{nl},r)}{r}$ where $Z_{eff}(\lambda_{nl},r) = Z[e^{-Zr/2} + \lambda_{nl}(1-e^{-Zr/2})]$ and λ_{nl} are the Thomas-Fermi scaling parameters for each orbital. The calculations include relativistic effects in Breit-Pauli approximation. The target wavefunctions are used as the input for the R-matrix suite of codes.

Solutions of the equation,

$$H^{BP}_{N+1}\Psi = E\Psi$$

for the (N+1) electron system which becomes a set of coupled equations with the CC expansion are bound wavefunctions, Ψ_B, for negative energies, E < 0, and continuun wavefunction, Ψ_F, for positive energies, E ≥ 0 (e.g. Seaton 1987).

c) Atomic Parameters in Astrophysical Models

The bound and continuum wavefunctions can be used to obtain the primary quantity the line strength for various bound-free radiative processes and scattering matrix for collision processes. The transition matrix elements for various atomic processes are:

$< \Psi_F|H(e+ion)|\Psi_{F'} >$ for electron impact excitation,

$< \Psi_B||\mathbf{D}||\Psi_{B'} >$ for oscillator strength of bound-bound transitions,

$< \Psi_B||\mathbf{D}||\Psi_F >$ for photoionization and recombination,

where $\mathbf{D}$ is the dipole operator, $\mathbf{D}_L = \sum_n r_n$, in length form and $\mathbf{D}_V = -2\sum_2 \Delta_n$ in velocity form, n is number of electrons.

i) Collision Cross Sections and Strengths for Electron Impact Excitations (EIE)

The radial asymptotic form of (N+1)th electron wavefunction, θ_i, is expressed as:

$$F_i(r) \sim_{r\to\infty} sin(\xi r) + cos(\xi r)\mathbf{K}, \tag{6}$$

where ξ is the Coulomb phase and $\mathbf{K}$ is the real *reactance* matrix. The *scattering matrix*, which is complex is given by $\mathbf{S} = (1 + i\mathbf{K})(1 - i\mathbf{K})^{-1}$.

The collision strength for electron impact excitation from an initial state of the target S_iL_i to the final state S_jL_j is given by (e.g. Seaton 1975)

$$\Omega(S_iL_i - S_jL_j) = \frac{1}{2}\sum_{SL\pi}\sum_{l_il_j}(2S+1)(2L+1)|\mathbf{S}^{SL\pi}(S_iL_il_i - S_jL_jl_j)|^2, \tag{7}$$

The effective collision strength or the Maxwellian averaged collision strength can be obtained as

$$\Upsilon(T) = \int_0^\infty \Omega_{ij}(\epsilon_j)e^{\frac{-\epsilon_j}{kT}}d(\epsilon_j/kT). \tag{8}$$

The collision cross sections Q for electron impact excitation is related to collision strength as

$$Q(i,j) = \frac{\Omega(i,j)}{g_ik_i^2}(\pi a_o^2), \tag{9}$$

where g_i is the statistical factor, $g = (2S+1)(2L+1)$ is LS coupling or $g = 2J+1$ in fine structure. Finally, the excitation rate coefficient is given by,

$$q_{ij}(T) = (8.63\times10^{-6}/\omega_iT^{1/2})e^{-E_{ij}/kT}\Upsilon(T)\ cm^3s^{-1}, \tag{10}$$

where T is in K, $E_{ij} = E_j - E_i$, $E_i < E_j$ are in Rydbergs (1/kT = 157885/T).

ii) Oscillator Strengths, Lifetimes, Photoionization, Opacities

The transition matrix element for a radiative bound-bound or bound-free transition with the dipole operator $\mathbf{D}$ can be reduced to the generalized line strength defined, in either length or velocity form, as

$$S_{\rm L} = \left|\left\langle\Psi_f|\sum_{j=1}^{N+1}r_j|\Psi_i\right\rangle\right|^2, \quad S_{\rm V} = \omega^{-2}\left|\left\langle\Psi_f|\sum_{j=1}^{N+1}\frac{\partial}{\partial r_j}|\Psi_i\right\rangle\right|^2. \tag{11}$$

where ω is the incident photon energy in Rydberg units, and Ψ_i and Ψ_f are the wave functions representing the initial and final states, respectively.

The oscillator strength f_{ij} for bound-bound transition from level i to j and the radiative decay rate or the transition probability A_{ji} from j to i can be obtained from S as

$$f_{ij} = \frac{E_{ji}}{3g_i}S, \quad A_{ji}(a.u.) = \frac{1}{2}\alpha^3\frac{g_i}{g_j}E_{ji}^2f_{ij}, \tag{12}$$

where α is the fine structure constant, g_i, g_j are the statistical weight factors. The lifetime of level j can be obtained from the sum of the decay rates to the lower levels as

$$\tau_j = \frac{1}{\sum_i A_{ji}(s^{-1})}, \quad A_{ji}(s^{-1}) = \frac{A_{ji}(a.u.)}{\tau_0}, \quad \tau_0 = 2.4191 \times 10^{-17} s. \tag{13}$$

The photoionization cross section (σ_{PI}) for bound-free transition is proportional to the generalized line strength (S),

$$\sigma_{PI} = \frac{4\pi}{3c}\frac{1}{g_i}\omega S. \tag{14}$$

The opacity gives a measure of radiation transport through plasmas. The monochromtic opacity is a function of the photon frequency and depends mainly on the detailed atomic data: bound-bound oscillator strengths and bound-free photoionization cross sections. Stellar models use Rosseland mean opacity, $\kappa_R(T, \rho)$, defined as (Seaton *et al.* 1994)

$$\frac{1}{\kappa_R} = \int_0^\infty \frac{1}{\kappa_\nu} g(u) du, \quad g(u) = \frac{15}{4\pi^4} u^4 e^{-u} (1 - e^{-u})^{-2}, \tag{15}$$

where g(u) is the Planck weighting function and $u = h\nu/kT$. Monochromatic opacities κ_ν depends primarily on oscillator strengths as

$$\kappa_\nu(i \rightarrow j) = \frac{\pi e^2}{mc} N_i f(ij) \phi_\nu \tag{16}$$

where N_i is ion density in state i, ϕ_ν is a profile factor, and on photoionization cross sections (σ_{PI}) as

$$\kappa_\nu = N_i \sigma_{PI}(\nu). \tag{17}$$

iii) Electron-Ion Recombination Cross Sections and Rates

The electron-ion recombination processes, radiative and di-electronic, are unified in nature. They can take place to infinite number of recombined states, bound or quasi-bound. The quasi-bound states are the resonant Rydberg series of states $S_i L_i (J_i) \pi_i \nu \ell$ belonging to various excited target or core thresholds $S_i L_i (J_i) \pi_i$. The existing methods treat the radiative recombination (RR) and the dielectronic recombination (DR) separately using different approximations that are valid in different temperature ranges and thus can introduce uncertainties when they are combined for the total. The new unified method for the total electron-ion recombination (Nahar & Pradhan 1992, 1994a, 1995) considers the infinite number of recombining states and incorporates the RR

and DR in a unified manner. The method divides the recombined states in to two groups. The contributions to recombination from group (A) states with $n \leq 10$ are obtained from detailed recombination cross sections σ_{RC}, while the resonant contributions from group (B) states with $10 < n \leq \infty$ are obtained from an extension (Nahar and Pradhan 1994a, Nahar 1996a) of the DR theory of Bell and Seaton (1985).

For group (A) state, the recombination cross section, σ_{RC}, is obtained from σ_{PI} through the principle of detailed balance,

$$\sigma_{RC} = \sigma_{PI} \frac{g_i}{g_j} \frac{h^2\omega^2}{4\pi^2 m^2 c^2 v^2}. \tag{18}$$

The recombination rate coefficient, α_{RC}, is obtained as

$$\alpha_{RC}(T) = \int_0^\infty v f(v) \sigma_{RC} dv, \tag{19}$$

where $f(v)$ is the Maxwellian velocity distribution function. The total α_{RC} is obtained from contributions of all individual states of group (A):

$$\alpha_R(T) = \sum_{i_b} \frac{g_i}{g_j} \frac{2}{kT\sqrt{2\pi m^3 k c^2 T}} \int_0^\infty E^2 \sigma_{PI}(i_b;\epsilon) e^{-\frac{\epsilon}{kT}} d\epsilon, \tag{20}$$

where $E = \hbar\omega = \epsilon + I_p$, ϵ is the photoelectron energy, and I_p is the ionization potential. As the photoionization cross sections of individual states include the detailed autoionizing resonances, the detailed balace provides the rate for both the RR and DR in a unified manner.

For the high-n group (B) states, DR dominates and the background RR is negligibly small. For these states, the recombining electron is treated as a 'spectator', recombining from an autoionizing level $\nu\ell$ to the corresponding $n\,\ell$ bound level following the ion core transition. Including radiative interactions in the total Hamiltonian for the e+ion system, Davies & Seaton obtained a generalized electron-photon scattering matrix $\mathcal{S}$ which includes all possible channels of electron, photon scatterings. From the unitarity condition, Nahar and Pradhan (1994a) derived the DR probability, P_α(DR), giving the DR collision strength, $\Omega(DR)$, as

$$\Omega(DR) = \sum_{SL\pi} \sum_{\alpha} \frac{1}{2}(2S+1)(2L+1) P_\alpha^{SL\pi}. \tag{21}$$

The $\Omega_{\rm DR}$ are calculated, in a self-consistent manner, using the same CC wavefunction expansion that is used for the calculation of $\sigma_{\rm PI}$. The DR cross section, in Megabarns (Mb), is related to the collision strength, $\Omega_{\rm DR}$, as

$$\sigma_{\rm DR}(i \rightarrow j)({\rm Mb}) = \pi \Omega_{\rm DR}(i,j)/(g_i k_i^2)(a_o^2 \times 10^{18}), \tag{22}$$

where k_i^2 is the incident electron energy in Ry. The contributions from these states are added to total recombination rates.

The unified method has two other inherent advantages in addition to the natural unification of resonant and non-resonant phenomena. It enables a general and self-consistent treatment of photoionization and electron-ion recombination employing idential wavefunction expansion and this reduces the uncertainties introduced in astrophysical models. The other advantage is that level-specific recombination rates can be obtained for a large number of bound states necessary for determinations of quantities such as level popolations.

iv) Ionization fractions in plasma equilibrium

One important application of self-consistent sets of atomic data for photoionization and electon-ion recombination is in determination of ionization fractions of elements in photoionization or collisional (coronal) equilibrium in astrophysical plasmas. Ionization fractions are crucial in finding various physical conditions of the plasma. The plasma is in coronal equilibrium where electon impact ionization is balanced by total electron-ion recombination or in photoionization equilibrium where the ionization by a radiative source is balanced by total electron-ion recombiation.

The relative concentrations of ions of a given element in coronal equilibrium are obtained by solving the ionization balance equation

$$N(z-1)S(z-1) = N(z)\alpha_{RD}(z), \tag{23}$$

together with the normalization condition

$$N_T = \sum_{z=0}^{z_{max}} N(z) \; and \; 1 \leq z \leq z_{max}, \tag{24}$$

where $N(z-1)$ and $N(z)$ are the densities for the recombining and recombined ions respectively, and $S(z-1)$ is the total rate coefficient for electron impact ionization from the ground state of the ion $X(z-1)$. $\alpha(z)$ is the total recombination rate coefficient as computed herein. The recombining ion is assumed to be in the ground state since the dominant stabilizing radiative transitions are to the ground state.

The ionization balance equation in photoionization equilibrium is

$$\int_{\nu_0}^{\infty} \frac{4\pi J_\nu}{h\nu} N(z-1)\sigma_{PI}(\nu, X(z))d\nu = N_e N(z)\alpha_R(z;T), \tag{25}$$

where σ_{PI} is the photoionization cross section evaluated at photon frequency ν, and convoluted by an isotropic radiation density J_ν of the source; N_e is the free electron density and ν_0 is ionization potential of the ion. The relative ionic fraction is obtained as

$$N(X^{i+})\left(\Gamma_i + N_e\alpha_i\right) = N(X^{(i+1)+})\Gamma_{i+1} + N(X^{(i-1)+})N_e\alpha_{i-1} \tag{26}$$

where $\Gamma(s^{-1}) = \int_{\nu_0}^{\infty} \frac{4\pi J_\nu}{h\nu}\sigma_{PI}(z,\nu)d\nu$ is the photoionization rate. Use of self-consistent data from the unified treatment for σ_{PI} on the left-hand-side, and α_{RC} on the right-hand-side, yields accurate ionization balance.

3 Results and discussion

Sample results for each atomic process and examples of some astrophysical applications are presented. Except for the oscillator strengths related to transition between two discrete bound energy levels, the cross sections and collision strengths show resonance structures because of formation of autoionizing states during the processes. Theoretically they are generated through overlapping integrals of bound and continuum states in the transition matrix elements.

a) Electron Impact Excitation (EIE)

The cross section for EIE is zero when the incident electron energy is below an excited threshold of the target. As the energy reaches to an excitation energy, the target is excited and the cross sections (Q) or the collision strength ($\Omega(EIE)$ rises. Fig. 1 shows an example such collision strength for electron impact excitation of Fe VI carried out by Chen & Pradhan (1999) under the IP. The electron energy is relative to the excitation threshold. The detailed collision strength $\Omega(E)$ showing extensive autoionizing resonances via couplings of channels, not considered in earlier investigations. Hence previous calculations seriously underestimate the Maxwellian averaged effective collision strength $\Upsilon(T)$ by several factors.

b) Oscillator Strengths, Transition Probabilities and Opacities

While the spectral lines of an ion can be identified from energy positions, the expected strengths are determined from the oscillator strengths (f) for excitation or transition probabilities (A) for

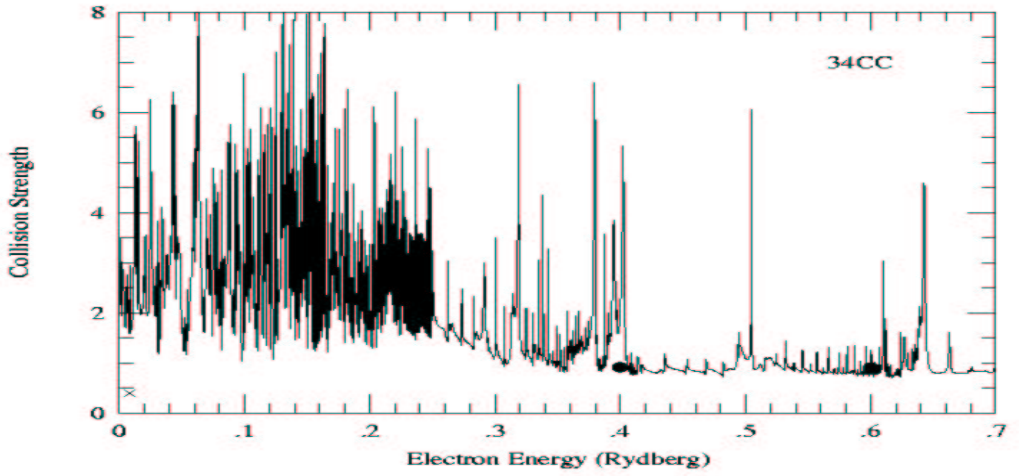

Figure 1: EIE oollision strength for the first transition in Fe VI $\Omega(^4F_{3/2} - {}^4F_{5/2})$ from the Iron Project (Chen & Pradhan 1999); previous results (• - Nussbaumer & Storey 1978, × - Garstang et al. 1978) neglect resonances.

de-excitation. Other processes such as photoionization, collisions as well as physical conditions of the plasmas may affect the intensities of the lines, but the dominant contributor of the intensities are these f and A values for the absorption and emission spectra. Plasma opacity depends largely on the all possible bound-bound transitions in the constituent atoms and ions requring extensive sets of such values. Fig. 2 shows monocrhromatic opacity of Fe II in a typical plasma:

In contrast to opacity, plasma diagnostics are carried out by a few well-separated lines of some elements. He-like ions are abundant in astrophysical plasmas and their four well known Kα lines, w, x, y, z are commonly used for X-ray diagnostics. These well separated lines are formed from transitions among the ground and the excited n = 2 levels $1s2p(^1P^o_1, {}^3P^o_{1,2})$, $1s2s(^3S_1)$, respectively and are observed easily. These lines are:

$$
\begin{aligned}
l1s^2\ (^1S_0) \longleftarrow 1s2p(^1P^o_1)\ &:\ w - dipole\ allowed(E1) \\
1s^2\ (^1S_0) \longleftarrow 1s2p(^3P^o_2)\ &:\ x - forbidden(M2) \\
1s^2\ (^1S_0) \longleftarrow 1s2p(^3P^o_1)\ &:\ y - intercombination(E1) \\
1s^2\ (^1S_0) \longleftarrow 1s2s(^3S_1)\ &:\ z - forbidden(M1)
\end{aligned}
$$

The types of transitions on the right are due to various multipole contributions. The electric dipole allowed (E1) includes both spin-allowed ($\Delta S = 0$) and intercombination ($\Delta S \neq 0$) transi-

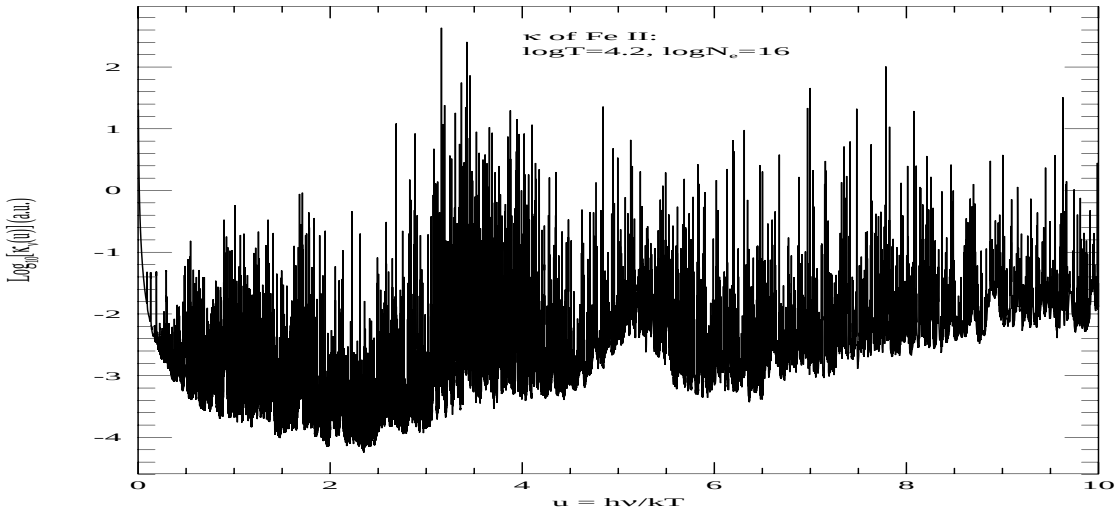

Figure 2: Monocrhomatic opacity of Fe II showing enhanced photoabsorption at frequency dependent quantity, $u = h\nu/kT = 5.5$ (Nahar & Pradhan 1994b).

tions. M1 and M2 are the forbidden magnetic dipole and magnetic quadrupole transitions (e,g, Nahar et al. 2003). Transition $1s^2\ (^1S_0) \longleftarrow 1s2p(^3P^o_0)$ decays by two or three photon radiation. The z-line gives a measure of plasma condition, such as recombining (strong z-line) or ionizing (weak z-line) plasmas. The formation of these X-ray lines due to recombination cascades from excited levels play an important role in determining the intensity ratios in coronal equilibrium and non-equilibrium plasmas.

c) Photoionization Cross Sections

The photoionization cross section (σ_{PI}) of the ground state of an atom or ion usually shows smooth background while the various features are observed for the excited states. Fig. 3 presents relatively simpler σ_{PI} of a highly charged nickel ion, He-like Ni XXVII. The ground $1s^2\ (^1S_0)$ level cross sections are in the topmost panel while the lower four panels present σ_{PI} of the four lowest n = 2 excited levels of Ni XXVII. The cross sections decay smoothly over a large energy range before appearances of resonance structures. The reason is the high energy position of the $n = 2$ excitation thresholds of core Ni XXVIII. The resonances correspond to Rydberg series of autoionizing states of LL and Ln ($n > 2$) complexes where K, L, etc are shell numbers. A sudden enhancement in σ_{PI} of the excited levels is seen at the n = 2 thresholds of the core. This jump

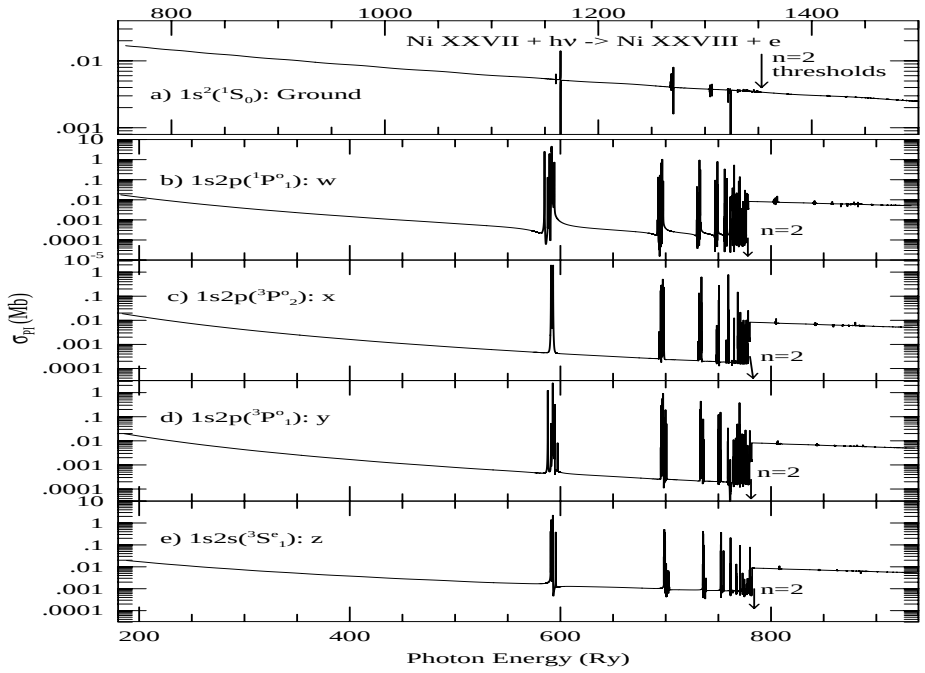

Figure 3: Photoionization cross sections of the ground and four excited levels of K_α lines of Ni XXVII (Nahar 2005).

is due to K-shell ionization via dipole allowed transition in the core levels, that is,

$$h\nu + Ni\ XXVII(1s2s, 1s2p) \longrightarrow e\ + Ni\ XXVIII(2s\ , 2p)$$

The excited levels correspond to the prominent lines w, x, y, z of Kα complex in the X-ray emission of He-like ions and yield valuable diagnostics of temperature, density, ionization balance, and abundances in the plasma source.

In addition to narrow Rydberg series of resonances, another type of prominent and wider PEC (photoexitation-of-core) resonances (Yu and Seaton 1987) can be seen in photoionization cross sections of excited states with a valence electron. A PEC resonance is manifested when the core goes through a dipole transition by absorbing the photon at energy equal to that for excitation while the outer Rydberg electron remains a 'spectator', weakly interacting with the core ion. Ultimately the core decays with ejection of the electon. Fig. 4 illustrates a PEC resonance in σ_{PI} of the Rydberg state, $3d^5 8s(^7S)$ of Fe III (Nahar 1996b). The arrow points the PEC resonance position at the energy of $^6P^o$ state of the core for transition $^6S -^6 P^o$.

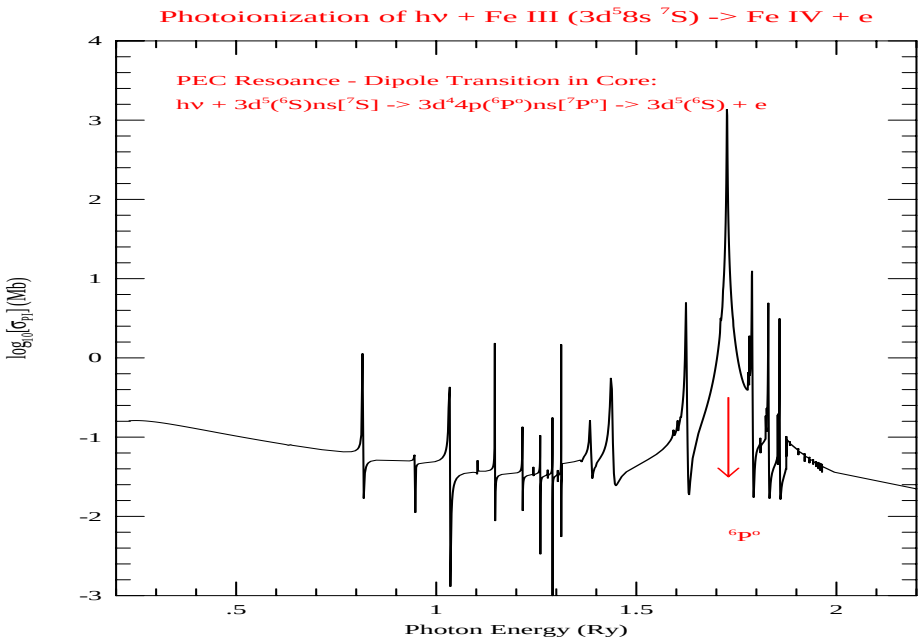

Figure 4: Photoionization cross sections of the excited $3d^8s(^7S)$ state of Fe III illustrating the PEC resonance (Nahar 1995).

d) Electron-Ion Recombination Cross Sections and Rates

Although photoionization cross section is studied for each state, the recombinaton cross section implies contributions from infinite number of recombined states. Fig. 5 presents unified electron-ion recombination cross sections, σ_{RC} for Ar XIV recombining to Ar XIII (Nahar 2004). The top panels shows σ_{RC} from about zero photoelectron energy to the highest core threshold beyond which no resonant structure is expected. The low energy cross sections are dominated by narrow Rydberg series of resonances belonging to n = 2 thresholds of the core. The peaks at the thresholds $2s2p^2(^2D,^2S,^2P)$ are mainly from DR contribution. The lower panel shows the recombination rates at photoelectron energies and can be measured at synchrotron experiements.

The total electron-ion recombination rate coefficient (α_{RC}) of an atom or ion is typically dominated by RR at lower temperatures and by DR at higher temperatures. Hence the basic feature is that it is maximum at low temperatures due to dominance by RR, decreases with temperature and rises again at very high temperatue due to dominance by DR beyond which it falls smoothly. However, a low temperature "bump" due to near threshold resonances (e.g. Nahar and Pradhan 1997) or multiple high temperature bumps due to enhanced resonant structures

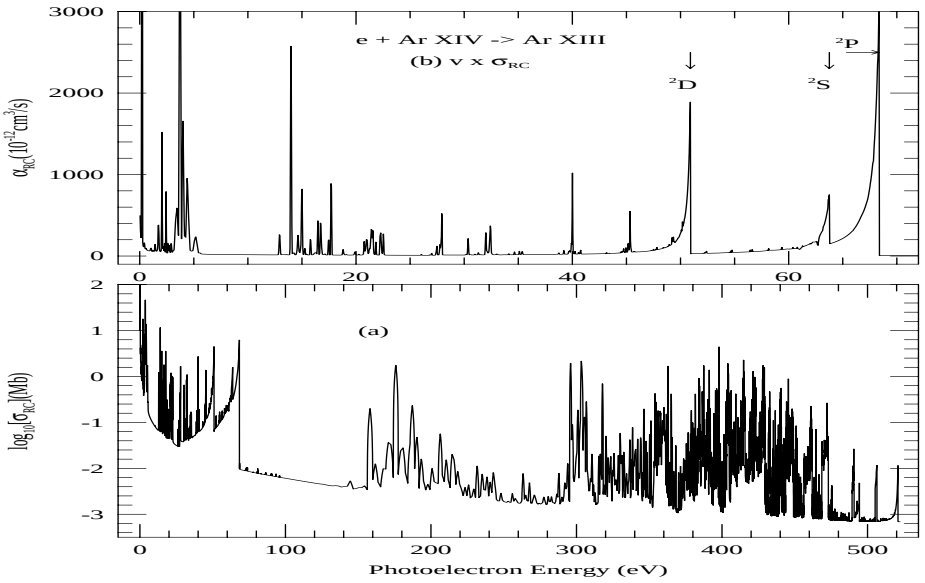

Figure 5: (a) The detailed unified σ_{RC} of Ar XIII in the energy range of n = 2 and 3 comlexes; (b) detailed recombination rate coefficient (v $\times\sigma_{RC}$) in the energy range of n = 2 complex. The dominant DR contributions can be seen below and at the core thresholds, ^2D, ^2S, and ^2P.

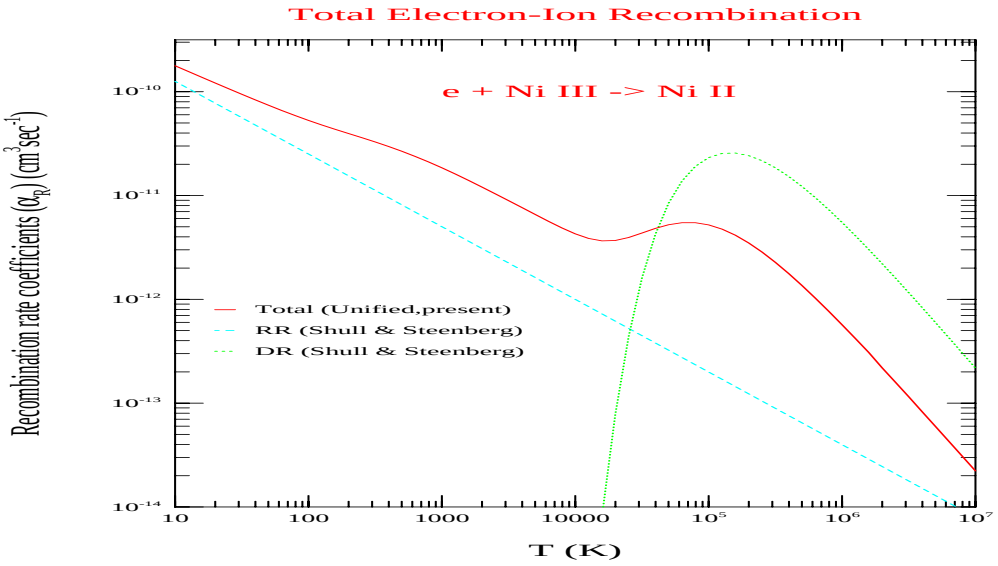

Figure 6: Total unified electron-ion recombination rate coefficients, $\alpha_R(T)$, for e + Ni III $\rightarrow$ Ni II (solid curve). The dashed curve is the RR and dotted curve is the DR rates by Shull and Steenberg (1982).

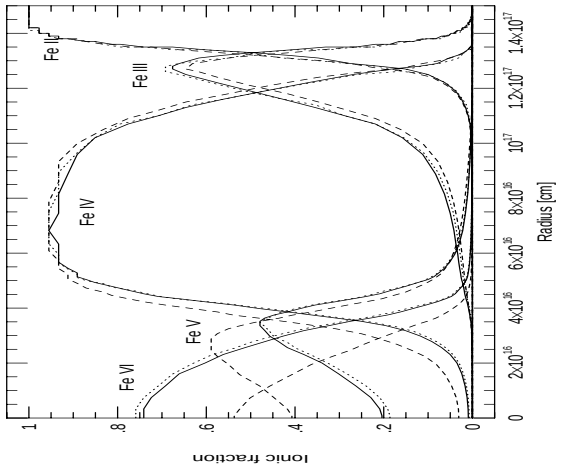

Figure 7: Ionization fractions of Fe II - Fe VI under typical physical conditions in a planetary nebula obtained using results from the OP and IP (solid curve) and from earlier calculations.

from strong dipole transitions to high core states (e.g. Nahar 2004) can also be seen. The basic pattern is seen in the total α_R of Ni II (e + Ni III $\rightarrow$ Ni II) in Fig. 6 (Nahar and Bautista 2001). A small "bump" in the low-temperature, at around 10^3K, is due to near threshold autoionizing resonances in the photoionization cross sections of Ni II. The earlier work on RR and DR rates by Shull and Steenberg (1982) employed simpler approximations for RR and DR rates. Their RR rate is underestmated since no resonances were included and DR from Burgess formula (1965) overestimates since autoionization channels to lower excited states were not considered.

e) Ionization Fractions

Ionization balance is the prime feature of astrophysical models of H II regions in general: diffuse and planetary nebulae, supernova remnants, and broad line regions of active galactic nuclei. The unified method is especially suited to this calculations. Fig. 7 shows the ionization structure of Fe ions in a planetary nebula under typical conditions: Solid curves are ionic fractions from new cross sections and recombination rates under the OP and IP; the dotted and dashed curves are from previous data. A large discrepancy is found for Fe V and Fe VI ionic fractions, by a factor of two at T_{eff} = 100,000 K.

4 Summary

A summary of the (i) dominant atomic radiative and collisional processes in astrophysical plasmas such as in stars, intergalactic medium, galaxies, active galactic nuclei, (ii) ab initio theories for the relevant atomic parameters, (iii) sample results for these processes, and (iv) examples of astrophysical applications are presented. We develop both the theoretical and computational methods to carry out large scale computations on Supercomputers for large amount of accurate atomic data as the astrophysical spectral analysis require consideration of large number of bound-bound, bound-free, and free-free transitions in the constituent ions. Most of the results presented have been obtained from ab initio close coupling R-matrix calculations and self-consistent unified treatment for total electron-ion recombination under the Opacity Project and the Iron Project.

Acknowledgements: This work is supported partially by the U.S. National Science Foundation and NASA.

References

[1] Bell, R.H. & Seaton, M.J. 1985, J. Phys. B 18, 1589.

[2] Berrington, K.A., Burke, P.G., Butler, K., Seaton, M.J., Storey, P.J., Taylor, K.T., & Yu, Yan, 1987, J.Phys. B, 20, 6379.

[3] Berrington, K.A., Eissner, W.B., & Norrington, P.H. 1995, CPC, 92, 290.

[4] Burgess, A. 1965, ApJ, 141, 1588.

[5] Burke, P.G. & Robb, W.D. 1975, Adv. At. Mol. Phys., 11, 143.

[6] Chen, G.X. & Pradhan, A.K. 1999, Astron. Astrophys. Suppl. Ser. 136, 395

[7] Davies, P.C.W., Seaton, M.J., 1969, J. Phys. B 2, 757

[8] Eissner W., 1991, in *The Effects of Relativity on Atoms, Molecules, and the Solid State*, p.55 (Edited by S. Wilson et al., Plenum Press, New York)

[9] Eissner, W., Jone, S. W., & Nussbaumer, N. 1974, CPC, 8, 270.

[10] Eissner W, & Zeippen C.J., 1981, J. Phys. B 14, 2125

[11] Hummer, D.G., Berrington, K.A., Eissner, W., Pradhan, A.K., Saraph, H.E., & Tully, J.A. 1993, A&A, 279, 298

[12] Nahar, S.N., 1996a, Phys. Rev. A, 53, 2417.

[13] Nahar, S.N., 1996b, Phys. Rev. A, 53, 1545

[14] Nahar, S.N., 2004, Astrophys. J. Suppl. 156, 93

[15] Nahar, S.N., 2005, Astrophys. J. Suppl. 158, 80

[16] Nahar, S.N., Bautista, M.A., 2001, Astrophys. J. Suppl. 137, 201

[17] Nahar, S.N., Eissner, W., Chen, G.X., & Pradhan, A.K., 2003, A&A 408, 789

[18] Nahar, S.N., Pradhan, A.K. 1992, Phys. Rev. Lett. 68, 1488

[19] Nahar, S.N., Pradhan, A.K. 1994a, Phys.Rev.A, 49, 1816.

[20] Nahar, S.N., Pradhan, A.K. 1994b, J. Phys. B, 27, 429

[21] Nahar, S.N., Pradhan, A.K. 1995, Astrophys. J. , 447, 966.

[22] Nahar, S.N., Pradhan, A.K. 1997, Astrophys. J. Suppl. , 111, 339.

[23] Seaton, M.J. 1975, Adv. Atom. Molec. Phys., 11, 83

[24] Seaton, M.J. 1987, J.Phys.B, 20, 6363

[25] Seaton, M.J., Yan, Yu., Mihalas, D., & Pradhan, A.K., 1994, Mon. Not. R. Astron. Soc. 266. 805

[26] Shull, J.M., van Steenberg, M. 1982, Astrophys. J. Suppl. , 48, 95.

[27] *The Opacity Project 1 and 2*, compiled by the Opacity Project team (Institute of Physices, London, UK, 1995, 1996)

[28] Yu Yan and Seaton, M.J. 1987, J. Phys. B, 20, 6409.